Wood Sci Technol (2012) 46:593–610
DOI 10.1007/s00226-011-0429-8

ORIGINAL

Strain fields around knots in Norway spruce specimens exposed to tensile forces

Jan Oscarsson · Anders Olsson · Bertil Enquist

Received: 10 June 2010 / Published online: 27 May 2011

Abstract Two-dimensional strain fields around knots in two Norway spruce specimens subjected to tension loading were detected using a contact-free measuring technique based on white-light digital image correlation. The first specimen included a traversing Edge knot, and the second one, a Centric knot. The development of strain fields as a function of load level was measured by consecutive cyclic load tests where one side of the specimen was studied during each test. The objectives were to examine to what extent the strain fields could be detected, to investigate the correlation between strain fields measured on different sides of a specimen and to analyse the strain distributions around the knots. The results show that the applied technique is useful for catching both overall and detailed information about the behaviour of knots in wood members exposed to loading. Clear wood defects that could not have been detected by neither visual inspection nor scanning were observed, and conclusions could be drawn regarding the release of internal stresses. The correlations between strain fields on different sides of the specimens were excellent, and the correspondence between measurement results and comparative finite element calculations was surprisingly good considering the fact that the employed FE models were fairly simple.

Introduction

Strength grading of structural timber means that strength, modulus of elasticity and density of individual timber members are predicted or measured by visual

J. Oscarsson (✉)
SP Technical Research Institute of Sweden, Videum Science Park, 351 96 Växjö, Sweden
e-mail: jan.oscarsson@sp.se

A. Olsson · B. Enquist
Linnæus University, 351 95 Växjö, Sweden

inspection or non-destructive machine testing. The market is, today, dominated by machine grading techniques that involve the determination of either flat-wise bending stiffness or dynamic stiffness in axial direction of a board. From previous research carried out by, *inter alia*, Johansson et al. (1992) and Larsson (1997), it is well known that the mentioned stiffnesses are, to a certain degree, correlated with the bending strength of a board. These relations are used to predict the latter property.

Present-day methods for machine grading result in a maximum characteristic strength of 40–45 MPa, but there are boards that in fact have a strength that exceeds 80 MPa. The reason why structural timber with characteristic strength higher than 45 MPa is not graded is that the prediction of a board's load-bearing capacity by the use of any available technique is not particularly good due to the somewhat limited correlation between stiffness and strength. Thus, to be able to utilize the potential of high strength timber, better grading methods are needed.

Mechanical properties of timber are, to a large extent, dependent on the occurrence of defects in the wood material. The degree of importance that different defects have on strength and stiffness has been investigated by, *inter alia*, Johansson et al. (1998) and Johansson (2003). It was found that knots were by far the type of defects that had the largest influence on visual grading and that the major cause of fracture was the presence of knots. Hence, it follows that a thorough knowledge and understanding of the behaviour of knots and the surrounding wood fibres in timber members exposed to loading is of great importance for the development of more accurate strength grading methods. Studies have been carried out concerning the effect of knots on the mechanical behaviour and mechanical properties of branch junctions. In an investigation carried out by Müller et al. (2006), it was found that the strain distribution of a mechanically loaded Norway spruce branch junction was very homogeneous, due to a combination of naturally optimized shape and optimized mechanical properties in the junction area. Jungnikl et al. (2009) measured the microfibril angle and density distribution at branch junctions of pine using computer tomography and X-rays, respectively, and found that the material properties vary locally as a response to different mechanical demands.

For studying the effect of knots on the strain distribution, techniques for contact-free deformation and strain measurement on surfaces of timber members could be useful. One such method, today widely used in, for example, the vehicle and aviation industries, is based on white-light digital image correlation (DIC). The use of DIC techniques in connection with wood or wood-based products is, however, rather limited. A review of research carried out up to the year 2005 is found in Serrano and Enquist (2005) where results from an investigation into strain distribution along wood adhesive bonds using DIC technique are presented. In recent years, the technique has been used for the measurements of, for example, strain in steel-to-timber dowel joints (Sjödin et al. 2006), strain in bi-axially loaded sheathing-to-framing connections (Vessby et al. 2008), strain distribution in timber subjected to four-point bending tests (Murata et al. 2005), strain-softening behaviour of wood under tension perpendicular to the grain (Miyauchi and Murata 2007) and tensile properties of early wood and late wood of loblolly pine (Young Jeong et al. 2009).

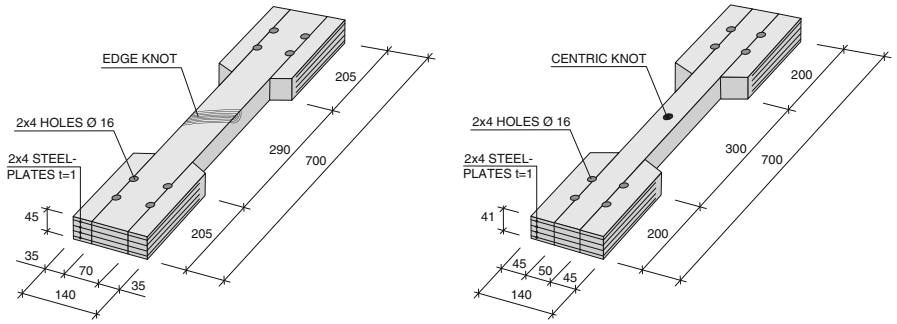

Fig. 1 Test specimens with Edge knot (*left*) and Centric knot (*right*)

Aim and scope

In this paper, findings from an investigation into two-dimensional strain fields around knots in wood members subjected to tensile forces are presented. Two test specimens of Norway spruce, one with a traversing Edge knot (henceforth denoted *Edge knot*) and one with a Centric knot (see Fig. 1), were studied using a non-contact optical 3D deformation measurement system of white-light DIC type. The aims were to examine 1. to what extent the strain fields could be detected, 2. the correlation between the strain fields measured on different sides of a specimen, and 3. the strain distribution around the knots. The development of strain fields was followed and measured by consecutive cyclic load tests consisting of both loading and unloading. Only one side of a specimen was studied during each test. Except for an initial test in which a crack in the Edge knot specimen widened and propagated, the loading was kept within the elastic range. Thus, the strain fields as a function of load level were detected in a comparable manner on all four sides of each specimen, even though only one side was studied during each test. The experimental results were also compared with those obtained from finite element (FE) simulations.

Test set-up and measurement equipment

The test set-up that was used for the experiments is shown in Fig. 2. The test specimens were fixed in a material testing machine of fabricate MTS with a 322 test frame, a control system of type FT60 and a maximum force capacity of ± 100 kN. The cyclic load that was applied during each test ranged from 0 to 30 kN, except for one test in which the maximum load was 40 kN. The load developed by the MTS machine was transferred to the test specimens by pin-ended steel yokes, each connected to the specimens by four steel dowels.

The two-dimensional strain fields in longitudinal and lateral directions and in shear occurring on the surfaces of the test specimens were detected using the measuring system ARAMIS^{TM}. It includes two charge-coupled device (CCD) cameras, in this case with a resolution of 2,048 $\times$ 2,048 pixels, placed in front of the specimen at angles and distances in accordance with a calibration procedure

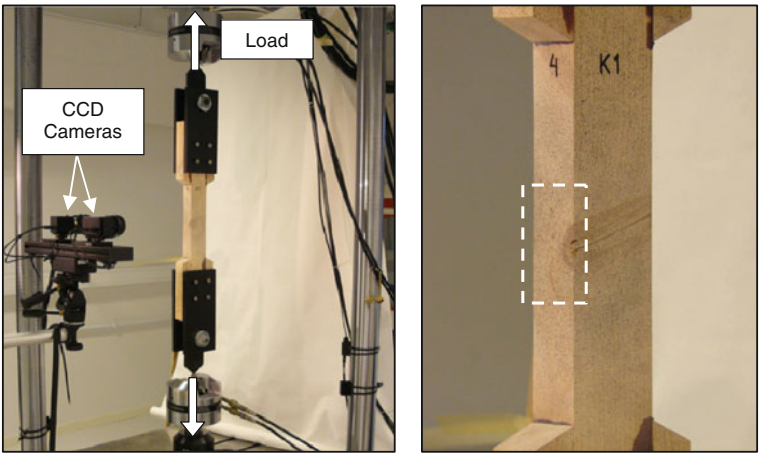

Fig. 2 Test set-up for the measurement of strain fields on one side of the Edge knot specimen (*left*) and corresponding measurement area (*right*)

carried out prior to the tests. With this equipment, strains in the range of 0.01–200% could be measured with an accuracy of up to 0.01% strain (GOM 2007).

During loading, the surface deformations and displacements are measured and recorded by pictures taken simultaneously, but from different angles, by the two cameras at fixed time intervals during the entire load test. Stereoscopic images are obtained from each pair of pictures, and current 3D-coordinates for a large number of points on the distorted surface are calculated relative to a coordinate system defined through the calibration procedure. In this research, pairs of pictures were taken at a time interval of 2 s, corresponding with a load increment of 400 N. Thus, each pair of pictures represents a unique load stage.

To be able to determine the displacements of a distinct point on the surface, each picture is divided into partially overlapping square or rectangular image subpictures, so-called facets. The size in pixels of both facets and overlap could be adjusted and chosen due to the spatial resolution and measurement accuracy needed for the test in question. In this case, the system's default settings, which are square 15 × 15 pixel facets and two pixel overlapping areas along the border of adjacent facets, see Fig. 3 (left), were chosen. This resulted in a facet step of 13 pixels, corresponding to a spatial resolution of about 0.67 mm. The default values are chosen as a compromise between measurement accuracy and computational time (GOM 2007). During a load test, each facet is identified for every subsequent stereoscopic image in the recording. This requires that the surface of the test object has an identifiable pattern, in this case a random speckled pattern of sprayed paint, see Fig. 3 (middle and right). During a test, the pattern deforms along with surface distortions, see Fig. 3 (right), and by the use of correlation algorithms, the 3D facet coordinates are calculated as the mean value of the coordinates of the facet corners. In Fig. 4, the coordinates of nine facets are shown as red and blue dots. These coordinates also define and coincide with the measuring point of the facet. Displacements of facet coordinates in a 3 × 3 facet mesh are used to calculate the strains in the measuring

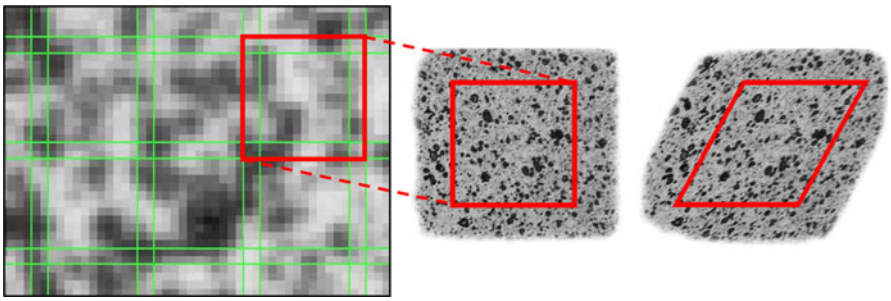

Fig. 3 Pixel facets of size 15 × 15 pixels with a two pixel overlap (*left*, GOM 2007), and random speckled pattern of a facet before loading (*middle*) and under loading (*right*)

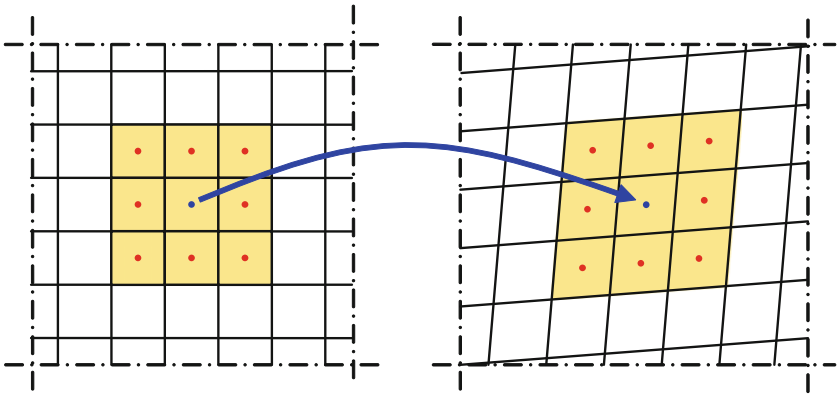

Fig. 4 Facet mesh before loading (*left*) and distorted facet mesh under loading (*right*)

point (blue dot in Fig. 4) of the centre facet of the mesh. By following the position changes of a large number of facets, the strain field as a function of load level can be determined and visualized.

Test specimens and loading

Drawings of the test specimens are shown in Fig. 1, and the dimensions and positions of the Edge knot and the Centric knot, respectively, are shown in Figs. 5 and 6. The experimental part of the research was divided into two test series, one for each test specimen. The Edge knot specimen was exposed to five load tests, numbered A0–A4, and the Centric knot specimen was exposed to four tests, numbered B1–B4.

In order to keep the stresses and strains within the elastic range, a maximum tension load of 30 kN was chosen for the Centric knot specimen, equal to an average tensile stress of about 15 MPa. For the Edge knot specimen, a higher load level was selected as the cross-section area of this specimen was more than 50% larger than the corresponding area of the Centric knot specimen. Since the presence

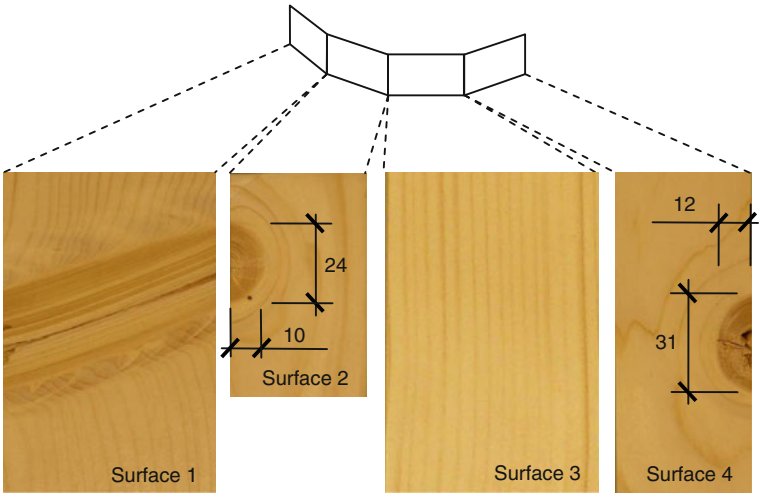

Fig. 5 Knot dimensions (mm) in Edge knot specimen

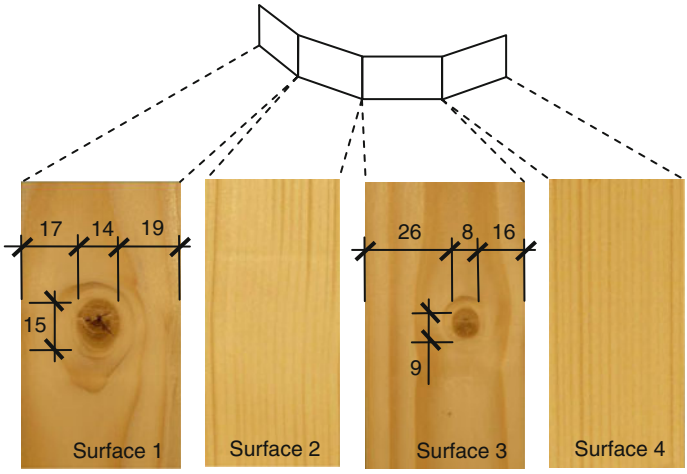

Fig. 6 Knot dimensions (mm) in Centric knot specimen

of the Edge knot caused a load eccentricity e of about 5.5 mm in the section through the knot, see Fig. 7 (left), the increase in the load level was limited to 10 kN resulting in a tension load of 40 kN for the Edge knot specimen. However, during the first load test (no. A0), an initial crack at the pith of the Edge knot expanded and propagated to the full depth of the knot, see Fig. 7 (left). Because of this, the load level was reduced to 30 kN, a load for which the strains on the surfaces of the Edge knot specimen were measured in tests A1–A4.

The load application in all tests was force-controlled, i.e., the load was both applied and detached with a constant load rate, in this case 200 Newton/s. The load–time relations for the different tests are shown in Fig. 7 (right).

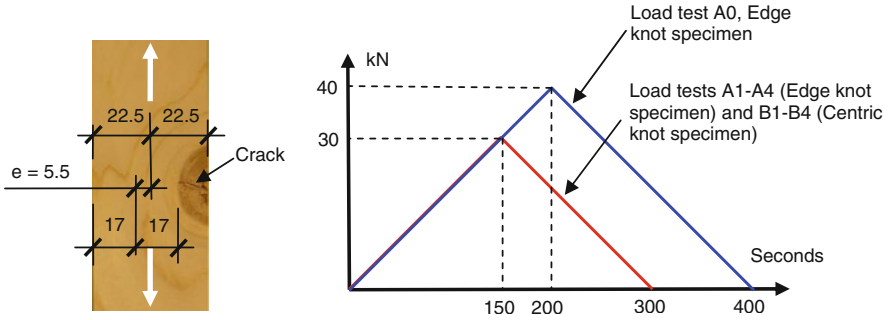

Fig. 7 Load eccentricity *e* (mm) in Edge knot specimen (*left*), and load–time relations for performed load tests (*right*)

Test results and evaluation

Two ARAMIS^{TM} post-processing tools, contour plots and section diagrams, were used to visualize the strain measuring results. By the first tool, a camera image of a measured surface is overlaid with coloured strain contour plots showing the strain distribution, for a defined load stage, over the measured surface. Such plots offer a qualitative and easily conceivable impression of the specimen's behaviour under loading. To obtain quantitative information with a higher degree of accuracy, sections can be defined in surface camera images and the strain variation along such sections can be shown in section diagrams. The position of a section is denoted in a local *xyz*-coordinate system defined in the camera image of each specimen surface. The results that are presented below concern the in-plane (*xy*-plane) strains that occurred on the surfaces of the test specimens. To be able to relate the four different coordinate systems on a specimen to each other, small marks of ink were applied on each surface. Since all marks were located at the same position in the longitudinal direction of a specimen and since the origin for each local coordinate system was located at such a mark, the measurement results for different surfaces of a specimen could easily be related to each other.

Load test no. A0: Edge knot specimen, load 40 kN

As described under the heading *Test specimens and loading* above, a tension load of 40 kN was chosen for this test where the strains on the specimen surface that shows a split section of the knot were measured, i.e. Surface 1 in Fig. 5.

Longitudinal strains (ε_y) for certain load stages are presented in Fig. 8. Stages 0–4 represent the undeformed and unloaded reference state, and the specified load level of 0.10 kN is considered as measuring noise. The load application started at stage 5 for which, at a load level of 0.59 kN, the widening of the initial crack in the pith of the knot is clearly visible.

Load stages 102–105 (see Fig. 8) illustrate the strain field just before and after the maximum load level of 40.1 kN was reached at stage 103. At this load, the crack had propagated and widened to such an extent that it was no longer possible to

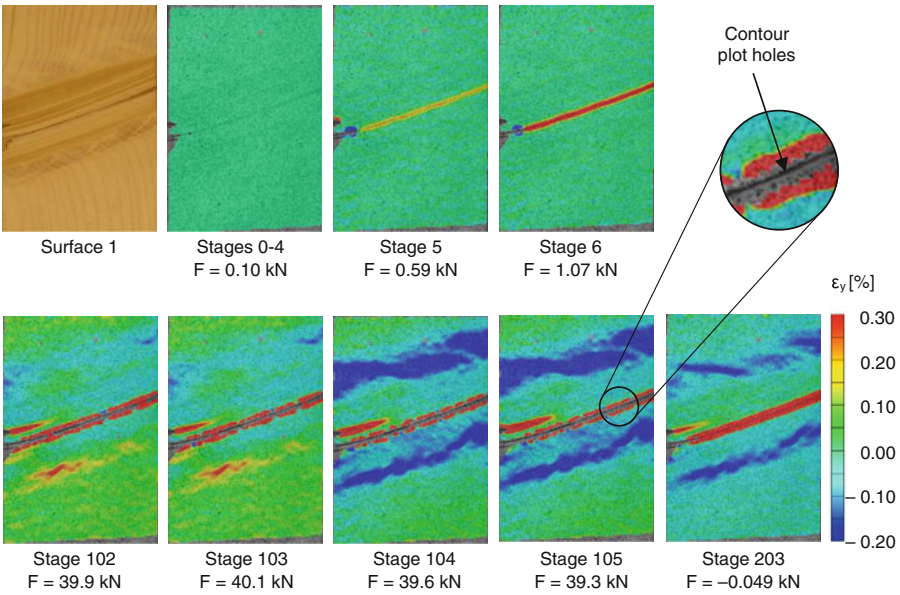

Fig. 8 Contour plots for longitudinal strains (ε_y) on surface 1, Edge knot specimen, load test no. A0, load stages no. 0–6, 102–105 and 203

identify displacements and deformations of facets in the crack area by means of the surface pattern of sprayed paint. Surface points that were not possible to identify are shown as holes in the contour plots, see detail in Fig. 8. During the unloading phase, the crack was gradually closed and the pattern restored to a degree where the facet displacements across the crack area were again possible to measure. However, considerable deformations, caused by crack propagation, remained in the crack after completed unloading at load stage 203. These deformations were represented by the ARAMIS^{TM} system as remaining longitudinal strains across the crack area, and they are shown as a thick red stripe in the contour plot for load stage 203, see Fig. 8.

In addition to the described crack deformations, large remaining negative (compressive) strains appeared in the wood fibres close to the knot. In general, strain changes measured by the ARAMIS^{TM} system from one load stage to another are rather small and more or less foreseeable, but in this test, the negative strains along the knot appeared instantly, at load stage 104, immediately after the maximum load of 40.1 kN was reached. During the 2 s that elapsed between the moments when pictures of load stages 103 and 104 were taken, the strain field was completely changed and areas of considerable negative strains emerged. A large portion of these remained after unloading, see load stage 203. A reasonable explanation for the sudden strain field changes is that crack growth during the test led to the release of internal stresses. After the test, the specimen was carefully examined and by using a pocket lens, two longitudinal clear wood cracks along the curvature of the fibre direction around the knot and one crack at the edge of the knot were discernible on Surfaces 2 and 4. The cracks are highlighted in the section diagrams of Figs. 9 and

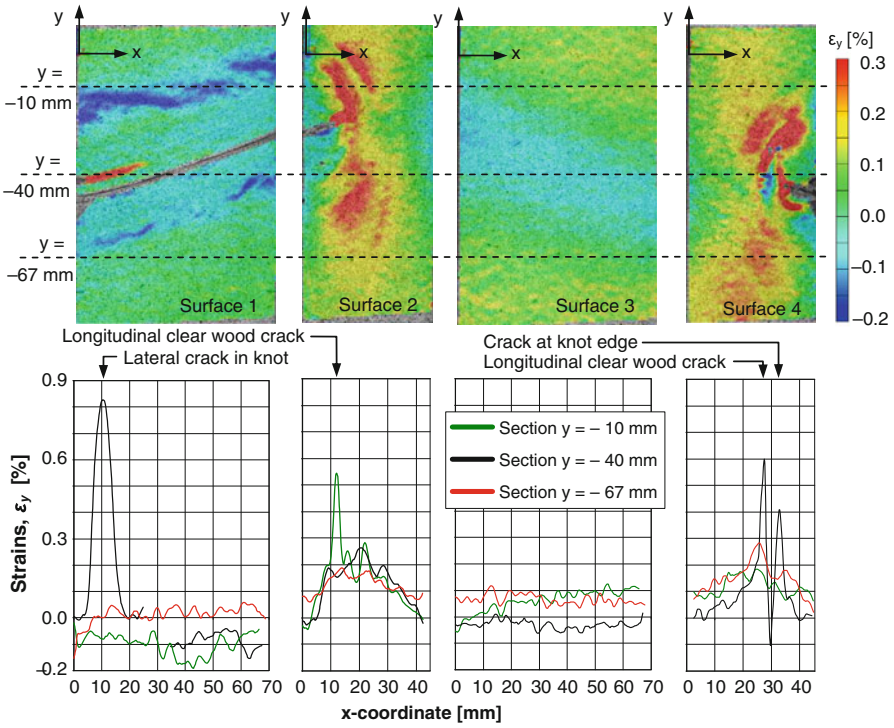

Fig. 9 Longitudinal strains (ε_y), Edge knot specimen, maximum load 30 kN, load tests A1–A4. *Top row* contour plots. *Bottom row* section strain diagrams for defined sections (*dashed lines*)

10. It should also be noted that the stress release occurred between the load stages 103 and 104, i.e. just *after* the maximum load level was reached. This indicates that the release was, to some extent, triggered by the change of sign of the load–time graph derivative, see Fig. 7 (right).

Load test no. A1–A4: Edge knot specimen, load 30 kN

In Load tests A1–A4, where the final strain stage of Load test A0 was used as unloaded reference stage (stage 0), the Edge knot specimen was exposed to a tension load of 30 kN for which the entire specimen displayed an elastic behaviour. Strain contour plots and section diagrams referring to the load stages for which the maximum load of 30 kN was reached are shown in Figs. 9 and 10.

The longitudinal strains (ε_y) are exhibited in Fig. 9. In spite of the fact that the specimen was exposed to tension loads, longitudinal negative strains were visible on Surfaces 1 and 3. The negative strains on Surface 1, measured during Load test A1, appeared in the same fibres as those where internal stresses were released in Load test A0. The appearance of these negative strains during Load test A1 was confirmed by a numerical analysis based on a 3D linear elastic model, see description under the heading "Numerical analyses" below. A possible explanation

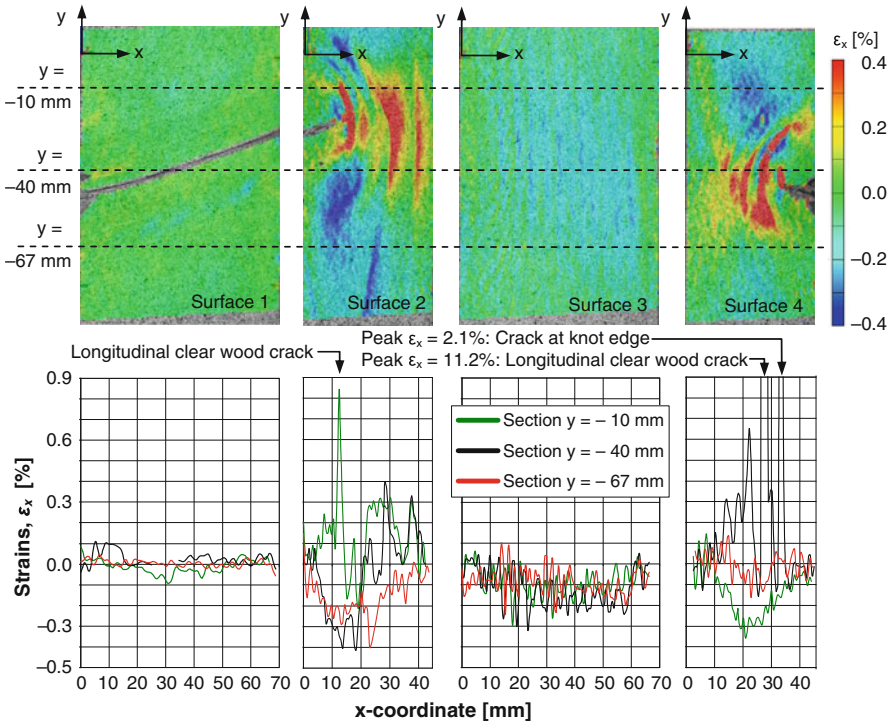

Fig. 10 Lateral strains (ε_x), Edge knot specimen, maximum load 30 kN, load tests A1–A4. *Top row* contour plots. *Bottom row* section strain diagrams for defined sections (*dashed lines*)

for this phenomenon is related to the behaviour of stress flow lines, i.e. imaginary lines showing how load is transferred between neighbouring material points. Such lines could be thought of as occurring in the vicinity of defects in specimens exposed to loading (Karihaloo 1995), and they create a biaxial stress and strain state. This effect is enhanced by deviating fibre directions around knots in timber members. The stress flow lines in the Edge knot specimen under tensile loading are exhibited in Fig. 11. The flow lines that develop under limited loading are shown as continuous lines. When the load increases, the eccentricity e shown in Fig. 7 creates a lateral deformation of the specimen that straightens the flow lines to the shapes represented by the dashed lines. From Fig. 11, the negative longitudinal strains occurring close to the knot on Surface 1 could be understood by studying the distances denoted a and b, measured between the tips of two lines drawn perpendicular to the flow line closest to the knot. The distance is reduced ($a > b$) when the line is straightened, and this may explain the negative strains in the clear wood fibres closest to the knot. The lateral deformation of the specimen, caused by the load eccentricity e, also explains the minor longitudinal negative strains in Section $y = -40$ mm on Surface 3, see Fig. 9.

The contour plots for Surfaces 2 and 4 in Fig. 9 exhibit large longitudinal tensile strains close to the knot. These strains are, like the strains discussed in the previous paragraph, related to the eccentricity e. Since hardly any stresses in the longitudinal

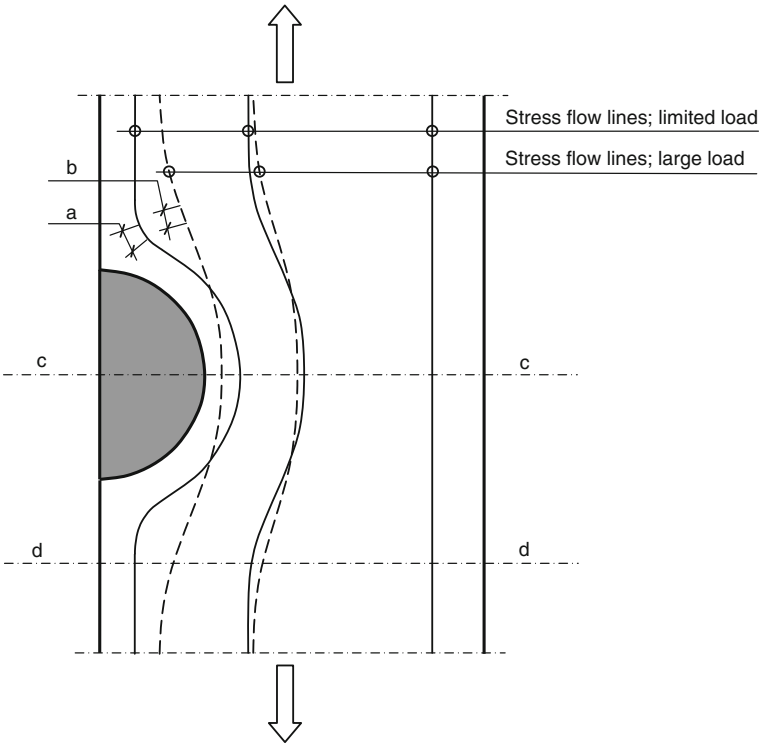

Fig. 11 Edge knot specimen under loading: straightening of imaginary stress flow lines

direction could be transferred through the knot, equilibrium requires higher longitudinal stresses and strains close to the knot than on the edge opposite to the knot. Furthermore, the fibre direction in the vicinity of the knot deviates considerably from the loading direction, and this difference probably contributes to increasing longitudinal tensile strains close to the knot.

The three strain peaks ($\varepsilon_y \geq 0.4\%$) in the section diagrams for Surfaces 2 and 4 in Fig. 9 are related to the previously described cracks that were observed by using a pocket lens. What is represented as surface strain peaks are, in fact, displacements caused by gradual widening of the cracks as load is applied.

A local tensile strain of about 0.82% was registered at Section $y = -40$ mm on Surface 1. As for the three strain peaks on Surfaces 2 and 4, this large strain value was also caused by the widening of a crack, in this case located within the knot and shown as a red stripe in the contour plot.

The lateral strains (ε_x) are presented in Fig. 10. They were insignificant on Surface 1, since the clear wood contraction was prevented by the presence of the knot. From a comparison of the contour plot of Surface 3 in Fig. 10 and the corresponding surface photo in Fig. 5, a correlation between the annual ring width and the wave-like pattern of the plot can be observed. This indicates a difference

between the Poisson's ratios of early wood and late wood of Norway spruce. Such a difference has been observed for loblolly pine by Young Jeong et al. (2009).

On Surfaces 2 and 4, lateral tensile strains developed beside the knot and compressive (negative) strains emerged in areas above and below the knot. As for the previously discussed longitudinal compressive strain shown on Surface 1, these lateral strains could also be understood from a study of the behaviour of the stress flow lines shown in Fig. 11. In section *c*, the lateral distance between the two flow lines that bend around the knot increases with increasing load and this indicates tensile strains in lateral direction. In section *d*, the lateral distance between the bending flow lines decreases corresponding to a lateral contraction. The huge apparent strains that coincide with the previously described cracks highlighted in the section diagrams in Fig. 10 are in fact lateral displacements caused by widening of the cracks.

Load tests no. B1–B4: Centric knot specimen, load 30 kN

Measurement results from tests carried out on the Centric knot specimen are shown in Fig. 12 (longitudinal strains, ε_y) and Fig. 13 (lateral strains, ε_x). All contour plots and section diagrams refer to the load stage for which the maximum load 30 kN was reached.

The contour plots for Surfaces 1 and 3 show large local strains, both longitudinal and lateral, in the vicinity of the knot. In the longitudinal direction (see Fig. 12), they could possibly and in a similar way as for the Edge knot be explained by a combination of stress flow line concentrations and deviation between fibre and loading directions. Regarding the strains in lateral direction, see Fig. 13, the expected contraction due to longitudinal tension loading is visible on both sides of the knot. The concentrations of large negative (compressive) lateral strains close to the knot are most likely caused by the curvature in the fibre directions and stress flow lines around the knot. The areas of tensile lateral strains visible above and below the knot on Surfaces 1 and 3 in Fig. 13 are similarly explained by an opposite curvature in fibres and stress flow lines.

From the lateral strain contour plots of Surfaces 2 and 4 in Fig. 13 and the photographs of the same surfaces shown in Fig. 6, the difference in Poisson's ratios between early wood and late wood is once again observed.

The contour plots and section diagrams in Fig. 12 reveal a concentration of longitudinal tensile strains in a section 20 mm below the local x-axis on Surface 4. According to the corresponding section diagram, there are strains as large as 0.95%, which is highly improbable. From the contour plots in Figs. 12 and 14 (left), it should be noted that just above the area where the large longitudinal strains occur, there are two zones where the longitudinal strains are approximately zero. In the same section as the large longitudinal strains appear on Surface 4, there are also, on an even more local scale, extreme contractions and expansions measured in the lateral direction of that surface, see Figs. 13 and 14 (right). A microscopic picture of the relevant area is shown in Fig. 14 (middle) where grain disturbances along a line on the surface are displayed. What is actually seen is the free edge of a surface chip and the concentration of large apparent strains described above are caused by

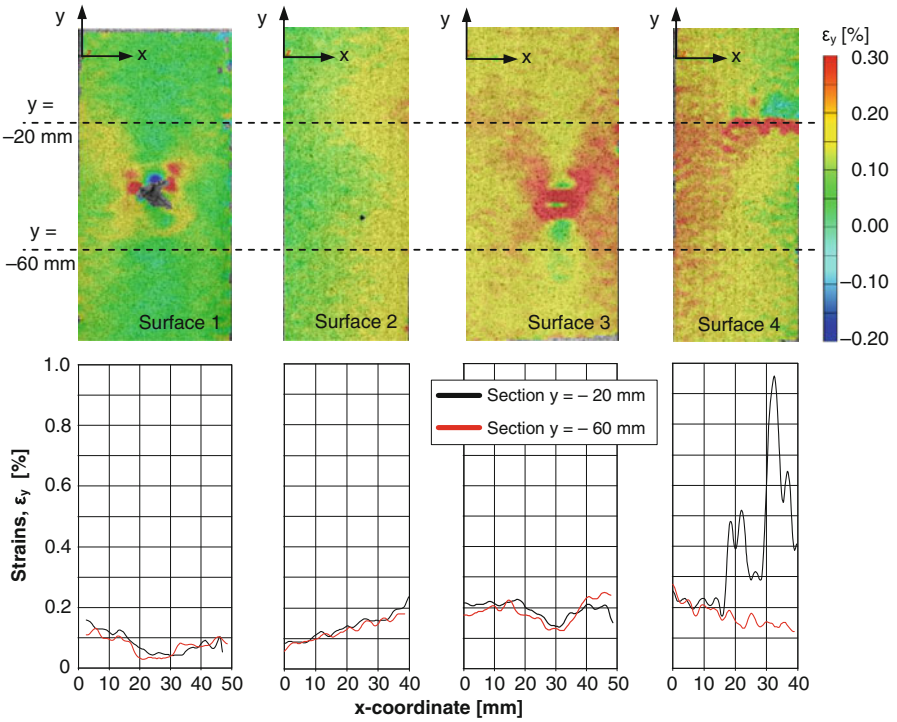

Fig. 12 Longitudinal strains (ε_y), Centric knot specimen, maximum load 30 kN, load tests B1–B4. *Top row* contour plots. *Bottom row* section strain diagrams for defined sections (*dashed lines*)

longitudinal and lateral translation of this edge. The presence of a chip clarifies why large apparent longitudinal strains are measured along a line on Surface 4 at the same time as there are large differences between the strains measured in areas on opposite sides of that line. The zero tensile strains in the area above the line are due to a rigid body translation of the chip.

Two more observations from Figs. 12 and 13 require comments. The first one concerns the fact that strains on both sides of a test specimen corner generally do not offer a perfect match. Computation of 3D coordinates and strain values for the measuring point of a facet requires that the previously described stochastic pattern of sprayed paint covers the entire area of the facet and that the entire pattern within the facet is visible from both the left and the right cameras. These requirements are not fulfilled for square facets that cover a corner of a test specimen. Consequently, on each side of a specimen corner, there are narrow areas where no strains could be calculated. However, with the exception of the corners themselves, the strain match between adjacent surfaces is very good considering the fact that they were established during different load tests. The second observation is that small areas of large lateral strains, both contraction and expansion, are found on the right-hand side of the contour plot of Surface 1 in Fig. 13. On this part of the specimen, the surface is rough due to minor maltreatment. According to the user manual for the

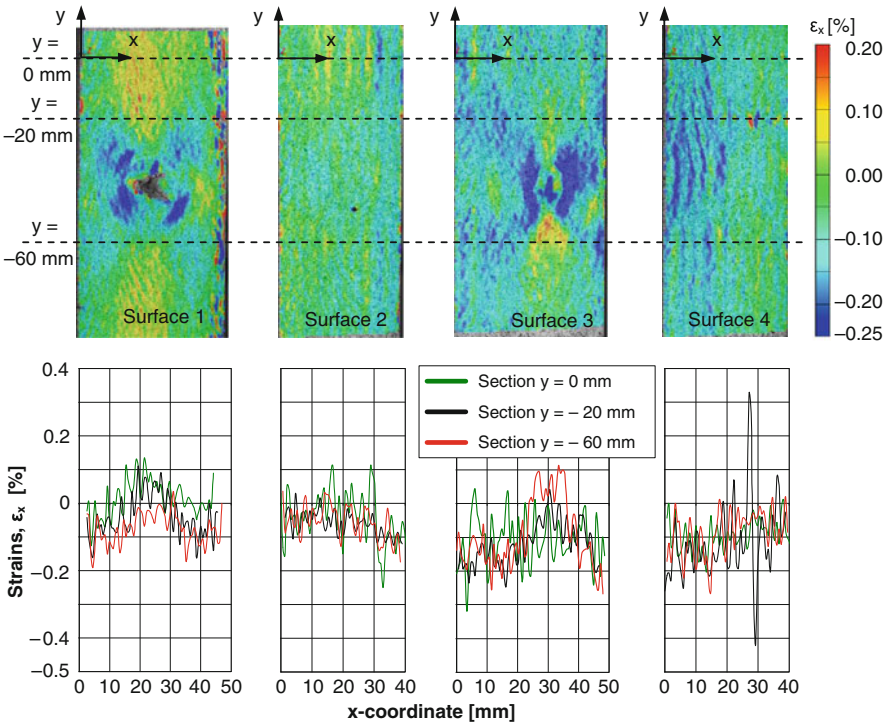

Fig. 13 Lateral strains (ε_x), Centric knot specimen, maximum load 30 kN, load tests B1–B4. *Top row* contour plots. *Bottom row* section strain diagrams for defined section (*dashed lines*)

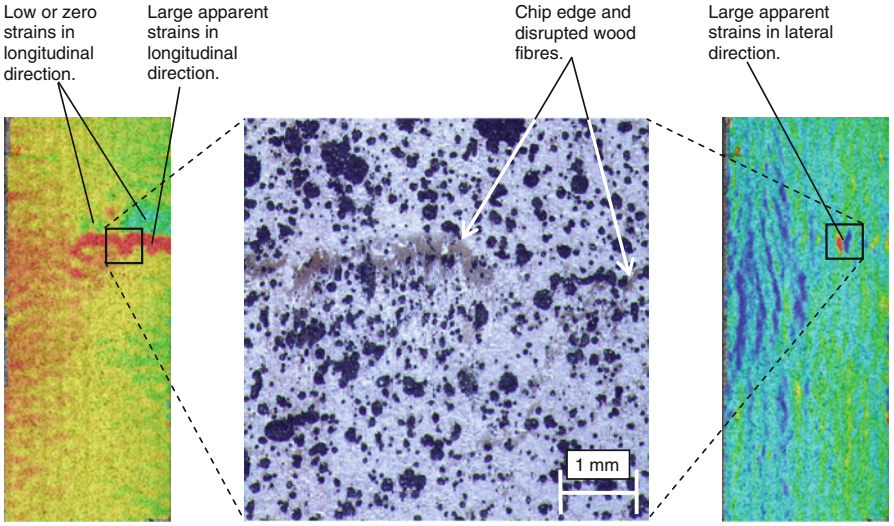

Fig. 14 Surface 4, Centric knot specimen: longitudinal strains (*left*), lateral strains (*right*) and microscopic picture showing disrupted wood fibres and chip edge (*middle*)

ARAMIS system (GOM 2007), an optimum specimen surface is smooth since highly structured surfaces may cause problems in facet identification and 3D point computation. Thus, the large strains identified on the rough part of the specimen surface are caused by incorrect measurement results and calculations.

Numerical analyses

The results of the experiments were compared with those obtained from FE simulations using the software ABAQUS (ABAQUS Inc. 2008). In the FE calculations, 3D linear elastic models of the test specimen's behaviour under loading were used. The model of the Edge knot specimen comprised about 113,000 2nd order elements and 483,000 nodes resulting in 1,449,000 degrees of freedom. Corresponding numbers for the Centric knot specimen model were 33,300 2nd order elements, 146,100 nodes and 438,200 degrees of freedom. In all simulations, a tension load of 30 kN was applied as a distributed load over the end surfaces of the specimens.

The material data needed for the numerical calculations, expressed in terms of elastic constants for spruce with a moisture ratio of 12%, were obtained from literature (Kollman and Côté 1968). The constants used for both clear wood and knots were $E_L = 13{,}500$, $E_R = 893$, $E_T = 481$, $G_{LR} = 716$, $G_{LT} = 500$ and $G_{RT} = 29$ MPa for the moduli of elasticity and the shear moduli and $\upsilon_{LR} = 0.43$, $\upsilon_{LT} = 0.53$ and $\upsilon_{RT} = 0.42$ for Poisson's ratios. The indices L, R and T refer to the longitudinal, radial and tangential directions, respectively, of the modelled orthotropic wood material. The longitudinal direction of the clear wood was oriented parallel to the longitudinal direction of the specimens, whereas the longitudinal direction of the knots was oriented perpendicular to the mentioned clear wood direction.

The applied FE models were fairly simple. The crack that widened and propagated in the pith of the Edge knot during load test no. A0 was included, but the material orientation deviations that always occur in clear wood close to knots were not regarded. Nevertheless, the simulation results presented in Figs. 15, 16 and 17 show, on an overall and qualitative level, a degree of correspondence with the experimental results shown in Figs. 9 and 10 and Figs. 12 and 13 that is surprisingly good. In terms of strain features on a closer level, several similarities deserve attention. For Surface 1 of the Centric knot specimen, calculated and measured strain fields in the vicinity of the knot strongly resemble one another, see Figs. 12, 13 and 15. This resemblance remains even if the knot is replaced by a hole, see Fig. 15, which is in accordance with assumptions made in, for example, the Nordic visual strength grading rules for timber, INSTA 142 (1998), namely that knots in structural timber should be equalized with holes (personal communication, Jan Brundin, SP Technical Research Institute of Sweden, 2008). INSTA 142 is referred to in the European Standard EN 1912 (2008) where nationally applied visual strength grades for visual grading of structural timber are assigned to common European strength classes established in the European Standard EN 338 (2003).

For the Edge knot specimen, the longitudinal negative strains measured on Surfaces 1 and 3, see contour plots in Fig. 9, could also be found in the

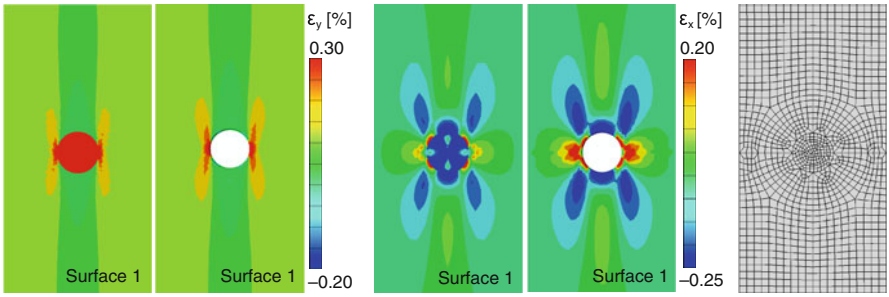

Fig. 15 Results from FE simulations, Centric knot specimen: longitudinal strains with and without knot (*left*), lateral strains with and without knot (*middle*) and FE mesh (*right*)

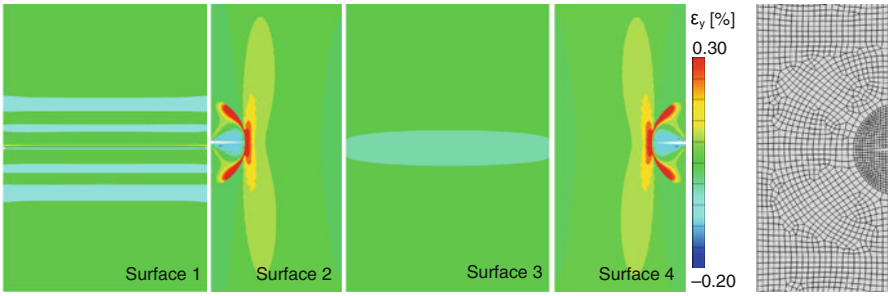

Fig. 16 Results from FE simulation, Edge knot specimen: longitudinal strains and FE mesh

corresponding plots in Fig. 16 and the areas of lateral compressive and tensile strains measured by the ARAMIS^{TM} system were also verified, see Fig. 17. However, the lateral strains are less evident in the FE simulations than in the ARAMIS^{TM} contour plots. The reason for this is probably that the curvature in the fibre direction around the knots increases the lateral strains measured on the surfaces of the test specimens, whereas no such effect is found in the FE calculations, since fibre curvatures are not included in the models.

The most conspicuous difference between measured and calculated strains concerns the large apparent tensile strains, both longitudinal and lateral, that occurred close to the knot in the Edge knot specimen. These apparent strains, which in fact were displacements caused by the cracks that were identified by using a pocket lens, could not be seen in the results of the simulations since these cracks were not included in the model.

Conclusion and future work

The objectives of this research were to investigate to what extent strain fields around knots could be detected by the use of DIC technique, to analyse the strain distribution around the investigated knots and to examine the correlation between

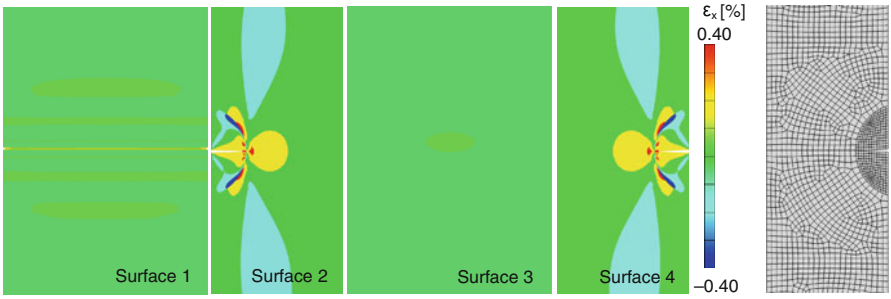

Fig. 17 Results from FE simulation, Edge knot specimen: lateral strains and FE mesh

the strain fields measured on different sides of a test specimen. Regarding the two first objectives, it could be concluded that the DIC technique is a useful tool for catching both qualitative and quantitative information about the behaviour of knots in wood members exposed to loading. The observation of release of internal stresses close to the knot in the Edge knot specimen must be considered as rather interesting. The graphical representations of the strain measuring results by the use of contour plots and section diagrams for different load stages in a load test provide valuable information about the strain distribution and development around knots. It is also possible to detect clear wood defects that are difficult to identify otherwise. For example, the chip on Surface 4 of the Centric knot specimen and the three cracks on Surfaces 2 and 4 of the Edge knot specimen could not have been detected neither by scanning nor by visual inspection. It is very likely that the discovered cracks will serve as indications of fracture and in the plans for future work, fracture tests are included. In such tests, the progress of fracture of the two specimens will be measured and documented by the use of the ARAMIS^{TM} system.

With reference to the objective concerning correlation between strain fields on different specimen surfaces, it has been demonstrated that the strain match between adjacent sides is very good, taken into account that only one specimen surface was measured during each load test.

Finally, the correspondence between the measurement results and the FE simulations is, indeed, promising, especially considering the fact that the applied models were rather simple. The DIC technique used in this research will, with a high degree of probability, be of great interest for the calibration of finite element models for, for instance, the analyses of fracture mechanical behaviour of knots in wood members. Such models would be of great importance for the development of more accurate strength grading methods based on scanned information concerning the occurrence of knots liable to initiate fractures in wood members to be graded.

Acknowledgments This research was made possible by the financial support from The Knowledge Foundation and The Swedish Research Council for Environment, Agricultural Sciences and Spatial Planning.

References

ABAQUS Inc. (2008) ABAQUS/Standard and ABAQUS/CAE version 6.8, User's manuals

European Standard EN 1912:2004+A2 (2008) Structural timber—strength classes—assignment of visual grades and species

European Standard EN 338 (2003) Structural timber—strength classes

GOM mbH (2007) ARAMIS User Manual—Software, aramis_v6_1st_en_rev-c, 25 April 2007

Inter-nordic standardisation INSTA 142/SS 23 01 20 (1998) Nordic visual strength grading rules for timber (in Swedish)

Johansson C-J (2003) Grading of timber with respect to mechanical properties. In: Thelandersson S, Larsen HJ (eds) Timber engineering. Wiley, Chichester, pp 23–43

Johansson C-J, Brundin J, Gruber R (1992) Stress grading of Swedish and German timber—a comparison of machine stress grading and three visual grading systems. SP Swedish National Testing and Research Institute, SP REPORT 1992:23

Johansson C-J, Boström L, Bräuner L, Hoffmeyer P, Holmqvist C, Solli KH (1998) Laminations for glued laminated timber—establishment of strength classes for visual strength grades and machine settings for glulam laminations of Nordic origin. SP Swedish National Testing and Research Institute, SP REPORT 1998:38

Jungnikl K, Goebbels J, Burgert I, Fratzl P (2009) The role of material properties for the mechanical adaptation at branch junctions. Trees 23(3):605–610

Karihaloo BL (1995) Fracture mechanics & structural concrete. Longman Group Ltd, Harlow

Kollman FFP, Côté WA (1968) Principles of wood science and technology. Springer, Berlin

Larsson D (1997) Mechanical characterization of engineering materials by modal testing. Dissertation D97:4, Chalmers University of Technology, Gothenburg

Miyauchi K, Murata K (2007) Strain-softening behaviour of wood under tension perpendicular to the grain. J Wood Sci 53(6):463–469

Müller U, Gindl W, Jeronimidis G (2006) Biomechanics of a branch-stem junction in softwood. Trees 20(5):643–648

Murata K, Masuda M, Ukyo S (2005) Analysis of strain distribution of wood using digital image correlation method—four-point bend test of timber including knots. Trans Visual Soc Jpn 25(9):57–63

Serrano E, Enquist B (2005) Contact-free measurement and non-linear finite element analyses of strain distribution along wood adhesive bonds. Holzforschung 59:641–646

Sjödin J, Serrano E, Enquist B (2006) Contact-free measurements and numerical analyses of the strain distribution in the joint area of steel-to-timber dowel joints. Holz Roh Werkst 64:497–506

Vessby J, Olsson A, Enquist B (2008) Contact-free strain measurement of bi-axially loaded sheathing-to-framing connection. In: Proceedings (CD) of the 10th world conference on timber engineering, Miyazaki, Japan

Young Jeong G, Zink-Sharp A, Hindman DP (2009) Tensile properties of earlywood and latewood from Loblolly Pine (Pinus Taeda) using Digital Image Correlation. Wood Fibre Sci 41(1):51–63